Fluorescence Correlation Spectroscopy analysis of segmental dynamics in Actin filaments

Anne Bernheim-Groswasser
Chemical Engineering Department, Reimund Stadler Minerva Center
and Ilse Kats Center for Nanoscience,
Ben-Gurion University, Beer-Sheva, Israel

Roman Shusterman
Physics Department
Ben-Gurion University, Beer-Sheva, Israel

Oleg Krichevsky [1]
Physics Department and Ilse Kats Center for Nanoscience,
Ben-Gurion University, Beer-Sheva, Israel

[1]Corresponding author. Address: Physics Department, Ben-Gurion University, Beer-Sheva, 84105 Israel, Tel.: (972)8647-2123, Fax: (972)8647-2904, Email: okrichev@bgu.ac.il

Abstract

We adapt Fluorescence Correlation spectroscopy (FCS) formalism to the studies of the dynamics of semi-flexible polymers and derive expressions relating FCS correlation function to the longitudinal and transverse mean square displacements of polymer segments. We use the derived expressions to measure the dynamics of actin filaments in two experimental situations: filaments labeled at distinct positions and homogeneously labeled filaments. Both approaches give consistent results and allow to measure the temporal dependence of the segmental mean-square displacement (MSD) over almost five decades in time, from $\sim 40\mu$s to ~ 2s. These noninvasive measurements allow for a detailed quantitative comparison of the experimental data to the current theories of semi-flexible polymer dynamics. Good quantitative agreement is found between the experimental results and theories explicitly accounting for the hydrodynamic interactions between polymer segments.

*Key words:*polymer dynamics, fluorescence correlation spectroscopy, F-Actin, semi-flexible polymers

Introduction

Living cells have remarkable mechanical properties which enable them to move, divide and respond to external stresses. These properties are mainly attributed to the dynamical characteristics of the cell cytoskeleton, which is a complex three-dimensional network of protein filaments mostly comprised of F-actin and microtubules. Both types of filaments are the polymerized forms of monomeric protein subunits: globular actin (G-actin) and tubulin, respectively. The cytoskeleton derives its strength from the elastic properties of these biopolymers, which, unlike synthetic polymers, are characterized by a high bending rigidity.

The polymer rigidity is described by a persistence length l_p above which thermal fluctuations can efficiently bend the polymer. Semi-flexible polymers such as F-actin and microtubules have a long persistence length: $l_p \sim 17\mu$m for F-actin (1) and several millimeters for microtubules, orders of magnitude larger than those of synthetic polymers. The large rigidity of these biological polymers enables us to experimentally address the fundamental questions of polymer dynamics at the sub-persistence length scales. The dynamics and the mechanical properties of F-actin and microtubule networks were studied by different optical techniques, such as dynamic light scattering (2), fluorescence imaging (3, 4), diffusive wave spectroscopy (DWS) and microrheology (5, 6, 7, 8, 9).

One of the most detailed features of polymer dynamics accessible in experiments is the kinetics of monomer motion measured by the temporal dependence of monomer's MSD $\langle r^2(t) \rangle$. For length scales below the persistence length, the monomer displacements are anisotropic with a major contribution coming from the transverse modes (displacements perpendicular to the polymer contour) and only a minor contribution from longitudinal modes. Theories (10, 11, 12, 13, 14, 15, 16, 17) predict that the kinetics of transverse motion, and thus the overall monomer's MSD, should follow the power law dependence of $\langle r^2 \rangle \propto t^{3/4}$.

A feature related to the monomer MSD, the time-dependence of the longitudinal fluctuations was obtained by measuring the end-to-end distance of individual actin filaments visualized by fluorescence video-microscopy (4). Although the data are consistent with theoretically predicted dependence, the temporal resolution of video-microscopy limits the measurements to time scales larger than 80ms (4) and thus the overall range of $\langle r^2 \rangle \propto t^{3/4}$ dependence spans over one order of magnitude in time only.

A wide range of time scales was assessed using DWS and microrheology of micron-sized beads inserted into the F-actin mesh (5, 8). The $\langle r^2 \rangle \propto t^{3/4}$

scaling was observed from $\sim 10\mu$s to ~ 10ms. However, it is not quite clear how the MSD of a bead is related to the actual monomers' displacements. While the beads' motion depends on the properties of the mesh, the beads themselves may affect the dynamics of the filaments, e.g. via their large friction coefficient (5). In particular, the monomer kinetics measured by fluorescence video-microscopy (4) is two orders of magnitude faster than the motion of the beads measured by DWS (5).

Here we present a new non-invasive approach to measure the monomer dynamics in stiff filaments: the filaments are tagged with fluorescent labels and the segmental dynamics of the filaments is then followed with Fluorescence Correlation spectroscopy (FCS) technique. We show that FCS correlation function is directly related to the temporal dependence of monomers' mean-square displacement (MSD) $\langle r^2(t) \rangle$. The measurement of the FCS correlation function allows us to obtain the kinetics of F-actin monomer motion over a wide range of time scales, from 40μs to 2s. Previously, the same method was used to study monomer dynamics in DNA polymers (18, 19). However, while the standard formulas of FCS can be applied to double-stranded DNA, new expressions relating FCS correlation function to monomer MSD have to be derived for stiff filaments such as F-actin and used to analyze experimental data. The main reason for that is the large difference in the persistence lengths of DNA and F-actin. In general, the dynamics of a semiflexible polymer is anisotropic: the segmental motions transverse to the filament are larger than longitudinal displacements. This anisotropy is lost at the length scales above polymer persistence length. For DNA, $l_p \approx 50$nm is much smaller than typical dimensions of FCS sampling volume (~ 500nm) and the expressions implying isotropic dynamics can be used in all of the dynamic range probed by FCS. For actin filaments with $l_p \approx 17\mu m$ the situation is reversed and the anisotropy of segmental motion has to be taken into account explicitly.

In the next section we derive the FCS expressions for anisotropic motion of stiff filaments. Although the segmental motion is dominated by the transverse component, for the sake of generality, we will derive the expressions which take into account explicitly both transverse and longitudinal displacements. Then we use these expressions to analyze the results of two sets experiments with different labeling strategies: 1) Partially (or locally) labeled filaments (obtained via polymerization of nonfluorescent monomeric actin on fluorescent seeds), and 2) homogenously labeled filaments (obtained by polymerization from a mixture of labeled and unlabeled actin monomers). The analysis of the experimental data with the expressions appropriate to each of the cases gives consistent results on temporal dependence of monomers

MSD. Finally, the experimental data are compared to theoretical predictions for the dynamics of semiflexible chains. The results are in qualitative and *quantitative* agreement with the theories taking into account hydrodynamic interactions between the polymer segments (12, 14).

Theory

FCS technique (20, 21, 22) (reviewed in e.g. (23, 24, 25, 26)) is based on monitoring fluctuations $\delta I_{em}(t) = I_{em} - \langle I_{em} \rangle$ in fluorescence emission $I_{em}(t)$ as fluorescence species diffuse in a spatially restricted excitation field, formed typically with the help of confocal optical scheme (27). The auto-correlation function $G(t) = \langle \delta I_{em}(0) \delta I_{em}(t) \rangle$ of emission fluctuations reflects the kinetics of motion of fluorescent sources.

In this section we adapt the general formalism of FCS to the case of dynamics of linear stiff polymers and derive expressions relating FCS correlation function to the temporal dependence of MSD $\langle r^2(t) \rangle$ of polymer segments.

The instantaneous detected emission, average emission and the correlation function of fluorescence fluctuations are found through the spatial distribution $c(\vec{r}, t)$ of fluorescent labels and excitation-detection profile $I(\vec{r})$ (21):

$$I_{em}(t) = Q \int d\vec{r} I(\vec{r}) c(\vec{r}, t),$$

$$\langle I_{em} \rangle = Q\bar{c} \int d\vec{r} I(\vec{r}), \tag{1}$$

$$G(t) = Q^2 \int d\vec{r} d\vec{r}' I(\vec{r}) I(\vec{r}') \langle \delta c(\vec{r}, 0) \delta c(\vec{r}', t) \rangle, \tag{2}$$

where Q is specific brightness of a fluorescent molecule dependent on fluorophore properties and the efficiency of detection optics, $\bar{c} = \langle c(\vec{r}, t) \rangle$ is the average concentration of fluorophores, and $\delta c(\vec{r}, t) = c(\vec{r}, t) - \bar{c}$. Following (28) Eq. 2 can be rewritten as:

$$G(t) = \frac{(2\pi)^3 Q^2}{V} \int d\vec{q} |\tilde{I}(\vec{q})|^2 \langle \delta \tilde{c}^*(\vec{q}, 0) \delta \tilde{c}(\vec{q}, t) \rangle, \tag{3}$$

where "tilde" denotes spatial Fourier transform of the corresponding quantities, such as e.g. $\tilde{I}(\vec{q}) = (2\pi)^{-3/2} \int d\vec{r} I(\vec{r}) e^{-i\vec{q}\vec{r}}$, and V is the total volume of the sample.

We assume that fluorescent molecules are not moving independently, but are attached to relatively large objects which themselves move independently of each other. We will further assume that the objects are statistically

equivalent and that the distribution of fluorophores within each object with respect to its center of mass is described by $\Phi(\vec{r}, \hat{s}(t))$, where $\hat{s}(t)$ denotes the set of internal degrees of freedom describing the current conformation and the orientation of the object. Then $c(\vec{r}, t) = \sum_j \Phi(\vec{r} - \vec{r}_j(t), \hat{s}_j(t))$, $\tilde{c}(\vec{q}, t) = \sum_j \tilde{\Phi}(\vec{q}, \hat{s}_j(t)) e^{-i\vec{q}\vec{r}_j(t)}$, where $\vec{r}_j(t)$ and $\hat{s}_j(t)$ define respectively the center-of-mass position and internal conformation of object j at time t. Finally, substituting these formulas in Eq. 3 we have:

$$G(t) = (2\pi)^3 Q^2 \bar{n} \int d\vec{q} |\tilde{I}(\vec{q})|^2 \langle \tilde{\Phi}^*(\vec{q}, \hat{s}(0)) \, \tilde{\Phi}(\vec{q}, \hat{s}(t)) \, e^{-i\vec{q}\Delta\vec{r}(t)} \rangle, \qquad (4)$$

where $\bar{n}$ is the average concentration of the objects (number of objects per unit volume), $\Delta\vec{r}(t) = \vec{r}_j(t) - \vec{r}_j(0)$ is the displacement of an object, and the index j was omitted everywhere in Eq. 4 due to the statistical equivalence of the objects.

In its general form Eq. 4 can be applied to any objects which have some internal structure and internal dynamics.

We assume now that the objects are uniformly labeled segments of semi-flexible polymers (one labeled segment per polymer, which, in general, are longer than their labeled parts and contain unlabeled parts). For sufficiently stiff polymers, we can neglect the dynamics within the labeled segments and consider them to be straight. In this case the set of internal degrees of freedom $\hat{s}$ reduces to a unit vector $\vec{s}$ defining the orientation of the segment. Within the same approximation we can assume that any given labeled segment moves without change in its orientation $\vec{s}_j(0) = \vec{s}_j(t)$. We will discuss in detail the validity of our assumptions at the end of this section. Here we just note that although these assumptions may look prohibitively restrictive, for sufficiently stiff filaments they are valid in a wide range of segmental displacements.

For a thin straight segment of length L uniformly labeled with linear density σ of fluorophores:

$$\tilde{\Phi}(\vec{q}, \vec{s}) = \frac{\sigma}{\pi\sqrt{2\pi}} \frac{\sin(\frac{1}{2} \vec{q}\vec{s} L)}{\vec{q}\vec{s}} = \frac{\sigma}{\pi\sqrt{2\pi}} \frac{\sin(\frac{1}{2} qL \cos\alpha)}{q \cos\alpha}, \qquad (5)$$

where α is an angle between $\vec{q}$ and $\vec{s}$. Furthermore, we split the segmental displacement into components parallel and perpendicular to the segment $\Delta\vec{r} = \Delta\vec{r}_{\parallel} + \Delta\vec{r}_{\perp}$, we assume the two components to be independent of each other and to be Gaussian random variables. Then, for fixed $\vec{q}$ and $\vec{s}$ the

ensemble average of $e^{-i\vec{q}\Delta\vec{r}(t)}$ is given by:

$$\langle e^{-i\vec{q}\Delta\vec{r}(t)}\rangle_{|\vec{q},\vec{s}} = \exp\left(-\frac{q^2\cos^2\alpha}{2}\langle\Delta r_\parallel^2\rangle - \frac{q^2\sin^2\alpha}{4}\langle\Delta r_\perp^2\rangle\right) \qquad (6)$$

The difference in the numeric prefactors in the two terms in the Eq. 6 stems from the fact that $\Delta\vec{r}_\parallel$ is defined on a line (parallel to $\vec{s}$), while $\Delta\vec{r}_\perp$ is defined in a plane (perpendicular to $\vec{s}$).

We assume, as it is usually done for confocal setups, the excitation-detection profile $I(\vec{r})$ to be 3D Gaussian axisymmetric with respect to optical axis Z:

$$I(\vec{r}) = I_0\exp\left(-\frac{2(x^2+y^2)}{w_{xy}^2} - \frac{2z^2}{w_z^2}\right) \qquad (7)$$

$$\tilde{I}(\vec{q}) = \frac{I_0 w_{xy}^2 w_z}{8}\exp\left(-\frac{w_{xy}^2}{8}q^2\sin^2\theta - \frac{w_z^2}{8}q^2\cos^2\theta\right), \qquad (8)$$

where w_{xy} and w_z define the width of the profile in the XY plane and in Z direction respectively, and θ is an angle between $\vec{q}$ and Z-axis.

Substituting (5),(6) and (8) into Eq. 4, averaging over α for a given $\vec{q}$ and integrating over $\vec{q}$, we have:

$$G(t) = \frac{\pi}{16}I_0^2 w_{xy}^5\omega^2 Q^2\sigma^2\bar{n}\int_0^\infty dk\int_{-1}^1 du\int_{-1}^1\frac{dp}{p^2}\sin^2\left(\frac{\lambda kp}{2}\right)\exp\left(-\frac{k^2}{4}f(h_\perp^2, h_\parallel^2, p, u)\right),$$
$$(9)$$

where $u = \cos\theta$, $p = \cos\alpha$, reduced units $k = qw_{xy}$, $\lambda = L/w_{xy}$, $h_\perp^2 = \langle\Delta r_\perp^2\rangle/w_{xy}^2$, $h_\parallel^2 = \langle\Delta r_\parallel^2\rangle/w_{xy}^2$ and $\omega = w_z/w_{xy}$ were introduced, and f denotes the following expression:

$$f(h_\perp^2, h_\parallel^2, p, u) = h_\perp^2 - p^2(h_\perp^2 - 2h_\parallel^2) + u^2(\omega^2 - 1) + 1 \qquad (10)$$

FCS correlation function is usually normalized by the square of the average emission $G_1(t) = \langle\delta I_{em}(0)\delta I_{em}(t)\rangle/\langle I_{em}\rangle^2$. With this normalization the amplitude of the correlation function at short time scales is the inverse of the average number N of molecules in the detection volume (given by $\pi^{3/2}w_{xy}^2 w_z$): $G_1(t\to 0) = 1/N$. Here we prefer another normalization: $G_2(t) = \langle\delta I_{em}(0)\delta I_{em}(t)\rangle/\langle I_{em}\rangle = \langle I_{em}\rangle G_1(t)$. A correlation function defined this way is independent of the concentration of the moving species (as long as there are no interactions between the objects) and its amplitude at short time scales gives the fluorescence per moving object: $G_2(t\to 0) = \langle I_{em}\rangle/N$. This is an interesting quantity in the context of labeled segments comparable or larger than w_{xy}: in this case only part of

the labeled segment can "fit" into the detection volume and contribute to the correlation function. The length of this part can be estimated from $G_2(t \to 0)$.

In order to calculate $G_2(t)$ we substitute $\bar{c} = \bar{n}\,\sigma L$ and (7) into (1) to find

$$\langle I_{em} \rangle = (\pi/2)^{3/2} I_0 w_{xy}^2 w_z Q \bar{n} \sigma L. \tag{11}$$

Performing integration over k in (9) and making use of (11) and of definition of G_2 we obtain:

$$G_2(t) = \frac{I_0 Q}{2\sqrt{2}} \sigma w_{xy} \frac{\omega}{\lambda} \int_0^1 du \int_0^1 dp \, \frac{1 - \exp(-\lambda^2 p^2 / f(h_\perp^2, h_\parallel^2, p, u))}{p^2 \sqrt{f(h_\perp^2, h_\parallel^2, p, u)}}. \tag{12}$$

Given the knowledge of the experimental geometry (i.e. parameters w_{xy}, w_z and L), Eq. 12 can be used to numerically calculate the relation between the FCS correlation function and temporal behavior of segmental MSDs, i.e. $h_\perp^2(t)$ and $h_\parallel^2(t)$.

In two important limiting cases the explicit expressions can be derived for $G_2(t)$: 1) for very short labeled segments, i.e. $L \to 0$ while $L\sigma = const$, and 2) for very long labeled segments, i.e. $L \to \infty$ while $\sigma = const$.

In the case of short segments, we obtain:

$$G_2(t) = \frac{I_0 Q}{2\sqrt{2}} \frac{\sigma L \omega}{\sqrt{(1 + h_\perp^2)(\omega^2 - 1)(h_\perp^2 - 2h_\parallel^2)}} \ln \frac{\sqrt{(1 + h_\perp^2)(\omega^2 + 2h_\parallel^2)} + \sqrt{(\omega^2 - 1)(h_\perp^2 - 2h_\parallel^2)}}{\sqrt{(1 + 2h_\parallel^2)(\omega^2 + h_\perp^2)}}$$

$$\tag{13}$$

We note that for isotropic motion, i.e. for $h_\perp^2 = 2h_\parallel^2 = \langle \Delta r^2 \rangle / (3 w_{xy}^2)$, the Eq. 13 reduces to the more standard FCS expression for the random motion of point-like objects:

$$G_2(t) = \frac{Q I_0}{2\sqrt{2}} (\sigma L) \left(1 + \frac{2}{3} \frac{\langle r^2(t) \rangle}{w_{xy}^2} \right)^{-1} \left(1 + \frac{2}{3} \frac{\langle r^2(t) \rangle}{w_z^2} \right)^{-1/2}. \tag{14}$$

For infinitely long segments Eq. 12 gives:

$$G_2(t) = \frac{Q I_0}{2\sqrt{2}} \frac{\sigma w_{xy} \omega \sqrt{\pi}}{\sqrt{(\omega^2 - 1)(1 + h_\perp^2)}} \arctan \sqrt{\frac{\omega^2 - 1}{1 + h_\perp^2}}. \tag{15}$$

Note that $G_2(t)$ in this case is independent of $h_\parallel^2$ since longitudinal motion of infinitely long labeled segments does not lead to any fluctuations in

fluorescence.

Although unrelated to our experiments, still an interesting particular case of application of Eq. 15 is that of spherically symmetric detection volume $w_{xy} = w_z = w$. In this case $G_2(t) = \sqrt{\pi/8}\, QI_0w\sigma(1 + h_\perp^2)^{-1}$ is similar to the correlation function produced by a planar motion of point-like objects.

We return now to Eq. 12 in order to find the dependence of the fluorescence per moving object $G_2(t \to 0)$ on the length of the labeled segment. We make use of the fact that for small segments $L \ll w_{xy}$: $G_2(t \to 0) = QI_0\sigma L/(2\sqrt{2})$, and define an apparent length L_{app} and respectively $\lambda_{app} = L_{app}/w_{xy}$ such that for the labeled segment of any length $G_2(t \to 0) = QI_0\sigma L_{app}/(2\sqrt{2})$.

For $t = 0$, i.e. $h_\parallel^2 = h_\perp^2 = 0$ it is possible to perform integration over u in Eq. 12 and arrive to the expression relating the apparent length of the labeled segment to its actual length and to the parameters of the detection volume:

$$\lambda_{app} = \frac{\omega}{\lambda\sqrt{\omega^2 - 1}} \left[-\ln(\omega + \sqrt{\omega^2 - 1}) + \int_1^\omega \frac{dv}{v\sqrt{v^2 - 1}} \left(\lambda\sqrt{\pi}\,\mathrm{erf}\left(\frac{\lambda}{v}\right) + ve^{-\lambda^2/v^2} \right) \right],$$

(16)

where $\mathrm{erf}(x) = 2\pi^{-1/2} \int_0^x e^{-t^2} dt$

An example of $\lambda_{app}(\lambda)$ dependence is shown in Fig. 1 for $\omega = 5$ corresponding to our experimental geometry. As expected for $\lambda < 1$, all of the segment can fit into the detection volume and $\lambda_{app} \approx \lambda$). For $\lambda \gg 1$ the apparent length saturates at the value which can be found from (15):

$$\lambda_{app}(\lambda \to \infty) = \omega\sqrt{\frac{\pi}{\omega^2 - 1}} \arctan\sqrt{\omega^2 - 1}. \tag{17}$$

Finally, we discuss the validity of assumptions leading to Eq. 12. The main assumption we made was to neglect the internal dynamics within the labeled segment. This assumption in fact just puts a lower limit on the accessible range of studied segmental displacements: the derived equations are valid as long as the center-of-mass motion $\Delta\vec{r}(t)$ of the segment is larger than the characteristic motions *within* the segment.

The characteristic internal motions $\langle \Delta r_{int}^2 \rangle$ within the labeled segment can be estimated to be of the order of $\langle \Delta r_{int}^2 \rangle = (2/45)L^3/l_p$ (14). For segmental displacements larger than that, motions *within* the labeled part can be neglected and the labeled segment can be considered essentially rigid and moving as a single unit.

This condition seemingly prohibits studies with long labeled segments, which have considerable motions within them. However, only a small part

of the filament (of length $\approx L_{app} < L$) can cross the sampling volume and contribute to the fluctuations in fluorescence at any given moment. Thus the lower limit for the range of accessible segmental motions can be further relaxed to $(2/45)L_{app}^3/l_p$. E.g. even for very long homogeneously labeled actin filaments ($L \gg w_{xy}$, $L_{app} \approx 2.5w_{xy}$) the segmental dynamics can be studied in the range $\langle \Delta r^2 \rangle > 4 \cdot 10^{-4} \mu m^2$.

The expressions derived in this section (such as Eqs. 12, 13, 15) can be directly used to measure segmental displacements from FCS correlation functions: only the parameters defining the experimental geometry (w_{xy}, w_z and in the case of Eq. 12 L in addition) need to be calibrated. All other parameters affect $G_2(t \to 0)$, the value of which can be determined from the plateau level of the experimentally measured correlation function at short time-scales. Finally, for the case of internal dynamics of a semi-flexible chain, relevant to most of the studies on actin dynamics as well as to our studies presented here, the longitudinal displacement $h_\parallel^2$ can be neglected in comparison to transverse motion $h_\perp^2$. Then, with known geometrical parameters and measured $G_2(t \to 0)$, Eq. 12 and its limiting cases Eqs. 13 and 15 give a one-to-one relation between segmental MSD and FCS correlation function. Some examples of such dependence are given in Fig. 2. Using these dependencies, the experimentally measured correlation function $G_2(t)$ can be converted into the temporal dependence of segmental MSD $\langle \Delta r_\perp^2(t) \rangle$ ($= w_{xy}^2 h_\perp^2(t)$).

Materials and Methods

Actin preparation

Unlabeled actin is purified from chicken skeletal muscle acetone powder and stored in G-buffer (29). Two sets of samples are prepared: 1) filaments labeled at defined positions, and 2) homogenously labeled filaments.

In order to label the filaments at defined positions (sample 1), we utilize fluorescently labeled actin filament seeds as templates for additional polymerization of unlabeled actin monomers. To prepare fluorescent seeds we first polymerize 1μM of fluorescent G-actin (Actin Alexa 568, Molecular Probes, Eugene, OR, or Rhodamine-Actin, Cytoskeleton, Denver, CO) in the presence of phalloidin (Molecular Probes) to stabilize the filaments (1:1 actin to phalloidin molar ratio). The labeled filaments are then broken by a brief sonication and vigorous pipetting into short fragments (average length of $\sim$ 170nm, estimated by FCS see **Results and Discussion**). These fragments are then used as seeds for further polymerization of unlabeled G-actin

(9μM). Polymerization proceeds for 10 min at room temperature. We note that concurrent with polymerization, there is an ongoing annealing process (30) which both increases polymer length and creates multiply labeled filaments. Independent fluorescence microscopy observation confirms that at the beginning of the experiment about ten percents of filaments are labeled at two distinct positions (typically separated by more than 1μm), while the rest are single-labeled. Since the distance between the labeled portions of the double-labeled filaments is much larger than confocal radius (0.21 μm), the "cross-talk" between the labels can be neglected and the formalism derived in the preceding section can be applied.

The homogenously labeled filaments (sample 2) are prepared in a similar manner. The difference is that the seeds are prepared from a mixture of labeled and unlabeled actin monomers (1:9 molar ratio) and further polymerization proceeds with the same mixture.

This procedure results in actin filaments of several microns in length: $\sim 4\mu m$ on average at the beginning of the experiment and growing in the course of experiment to $\sim 8\mu m$ due to annealing, as verified by fluorescence microscopy.

For the experiments, the solution is diluted tenfold to a final actin concentration of 1μM. Typically, one microliter of solution is sealed between two glass coverslips separated by a 250μm spacer. To prevent protein adsorption, the glass coverslips are coated with an inert polymer (Polyethylene Glycol) according to the protocol of (31). Most of the measurements were carried out at a distance of 40μm from the surface. This distance was chosen on purpose to be larger than F-actin length in order to minimize the effect of surface proximity on filament dynamics. Control experiments performed at a distance of 100μm from the surface give results identical to those presented here.

The experiments are started immediately after dilution and are conducted within 30 minutes. The main reason to limit the duration of experiment is to minimize the effect of actin filament fragmentation, which leads to appearance of short filaments and associated noise in the FCS correlation function. After $\sim$1 hour of FCS measurement we start to see the changes in the MSD due to the fragmentation: the MSD vs. time curve shifts to larger displacements. To be on the safe side, we limit all of our measurements to the first 30 min after polymerization.

Experimental setup

The optical setup is home-built based on the Nikon Eclipse TE300 inverted microscope (Nikon Corporation, Tokyo, Japan). The confocal excitation is provided by 514nm line ($\sim 2.5\mu$W power before microscope objective) of an Ar-ion laser (Advantage 163D, Spectra-Physics, Mountain View, CA) deflected by Q525 dicroic beamsplitter (Chroma Technology, Rockingham, VT) into a high-power objective lens (UPLAPO 60X1.2W, Olympus Europe, Hamburg, Germany). The collected emission passes through the beamsplitter, then a bandpass filter HQ565/80 (Chroma Technology, Rockingham, VT) and a pinhole of $50\mu m$ in diameter. The emission is detected by a photon counting avalanche photodiode (SPCM-AQR-14 PerkinElmer Optoelectronics, Vaudreuil, Quebec, Canada) whose output is fed into digital correlator Flex2k-12Dx2 (Correlator.com, Bridgewater, NJ). The correlator is capable of working in two modes, either as traditional correlator carrying out the correlation analysis of emission online, or as photon history recorder, storing the time arrivals of every photon on computer hard drive. For the presented experiments, we make use of the photon history recorder mode, while analyzing the recorded photon traces offline with software correlator as described in **Data Analysis**. The correlator program was written as C-module running under MATLAB environment (MathWorks, Natick, MA).

The parameters $w_{xy} \approx 0.21\mu m$, $w_z \approx 1.1\mu m$ of the confocal volume are calibrated before and after each experiment by measuring the diffusion of free Rh6G fluorophores (27).

Data Analysis

Sample 1: The measurement of the photon emission count rate from locally labeled F-actin reveals that photons arrive in intense bursts of $\sim 10^5$ counts/sec lasting ~ 0.1 to 1s, separated by intervals of low count rate of $\sim 10^3$ counts/sec (Fig. 3). The bursts are caused by the passage of the labeled F-actin through the confocal volume. The fluorescence in between the bursts originates from residual free fluorophores diffusing in the sample. The motion of the free fluorophores results in a correlated background noise $I_b(t)$ which adds up with the labeled actin signal $I(t)$ to a total emission $I_{tot} = I + I_b$. Thus the overall correlation function $G_{tot}(t) = \langle \delta I_{tot}(0)\delta I_{tot}(t)\rangle$ is given by:

$$G_{tot}(t) = G(t) + G_b(t), \tag{18}$$

where $G(t) = \langle \delta I(0)\delta I(t)\rangle$ and $G_b(t) = \langle \delta I_b(0)\delta I_b(t)\rangle$ are the correlation functions of emission from labeled segments and from free fluorophores re-

spectively.

Although the overall contribution of free fluorophores G_b to the total correlation function is small, their fast motion is responsible for most of the decay of the correlation function at the time scales below 1ms, where the motion of the filament segments is negligible. This could limit the analysis of monomers' MSD to the time scales above 1ms. However, as shown below, it is possible to separate the contributions of labeled actin and free fluorophores within the *same* experiment, and thus, extend the range of measurements to time scales as low as $\sim 40\mu$s.

In order to separate free fluorophore noise from the signal, we record the complete photon trace, i.e. times between arrivals of consecutive photons (with temporal resolution of 16.7ns). The photons are then binned into 100ms intervals $\{I(t_n)\}$ (Fig. 3). The stretches of time with no bursts are determined and the background correlation function $G_b(t)$ is calculated on these stretches using the original photon traces. The total correlation function $G_{tot}(t)$ is computed using the complete photon trace. Finally, the contribution of labeled actin $G(t)$ is obtained using Eq. (18). The intensity-normalized correlation function of actin segments is found by $G_2(t) = G(t)/(I_{tot} - I_b)$.

We find this procedure more robust than the correlation analysis of bursts intervals. First, there is some background contribution within the bursts as well. Second, unlike bursts, the intervals of pure background can be determined unambiguously: any intervals suspect to contain a burst can be deselected.

Practically, the background is deduced by calculating the median intensity over all bins $I_{med} = median(\{I(t_n)\})$, and selecting all of the intervals which deviate from the median by less than $\sigma = median(\{(I(t_n) - I_{med})^2\})$ for analysis of background noise. An example of this procedure is presented in Fig. 3. The resulting total, background and signal correlation functions $G_{tot}(t)$, $G_b(t)$ and $G(t)$ are shown in Fig. 4. The background correlation function $G_b(t)$ is indeed well described by 3D diffusion model of the free fluorophore (27) with a characteristic decay time of 70μs. We note that the amplitude of $G(t)$ is much larger than that of $G_b(t)$ mainly due to the multiple labeling of the filament segments: thus the motion of the labeled segments leads to much larger fluctuations in emission than the motion of single fluorophore molecules.

For calculation of monomers' MSD the amplitude of the correlation function $G_0 = G(t \to 0)$ is estimated from the level of the correlation function in 3 to 20 μs range, which is above the characteristic time scales of the fluorophore triplet state kinetics and below the characteristic time scales of

segmental dynamics.

Sample 2: We use the same approach to analyze data from homogeneously labeled F-actin. However, since the passage of the labeled segments through the sampling volume is more frequent in this case as compared to Sample 1, we make use of shorter binning intervals of 30ms and we pick the intervals with the average count rate not exceeding $I_{med} + 0.25\sigma$ for the analysis of background noise. These conditions give a noise correlation function with characteristic decay time below $100\mu s$. The above parameters were found to be optimal between less restrictive conditions which lead to a notable contribution of the signal in the estimated noise correlation function (characterized by decay times exceeding 1ms), and more restrictive parameters which clearly underestimate the noise level.

Results and Discussion

We present the correlation functions obtained from both types of samples in Fig. 4. To facilitate the comparison of temporal kinetics, the amplitude of the correlation function of homogeneously labeled actin was adjusted to the level of the correlation function of the partially labeled sample. The functions look similar but are notably shifted in time: the correlation function of the homogeneously labeled sample decays slower by a factor of ~ 1.4 than that of the locally labeled F-actin.

We can estimate the length of the labeled parts of Sample 1 by analyzing the amplitude of its intensity-normalized correlation function $G_2(t \to 0)$. G_2 amplitude is 62 ± 8 times higher than the corresponding amplitude of the correlation function of G-actin monomers obtained in similar conditions (data not shown). Since 14 actin monomers form a filament of 37nm, this gives the apparent length of the labeled segment of $L_{app} \approx 160 \pm 20nm$. Converting L_{app} into real segment length (Eq. 16 or Fig. 1) we obtain $L \approx 170 \pm 30nm$.

The apparent length of *homogeneously* labeled F-actin is $\sim 470nm \approx 2.3w_{xy}$, as estimated from the amplitudes of the corresponding correlation functions. This value is in a good agreement with our expectations for long homogenously labeled filaments (Eq. 16 and Fig. 1).

As discussed above, in order to extract $\langle \Delta r_\perp^2(t) \rangle$ dependence from the correlation functions we neglect longitudinal motion of the segments. Although the general expression Eq. 12 can be used to analyze both sets of data, the numerical calculation shows that for $L < w_{xy}$ (i.e. $\lambda < 1$) Eq. 12 leads to essentially the same dependence of the correlation function G_2 on

MSD as Eq. 13 derived for point sources (Fig. 2). Similarly, for homogeneously labeled filaments with length larger than $3\mu m$ ($\lambda > 15$), the Eq. 15 for infinitely long labeled segment can be used (compare curves for $\lambda > 15$ and $\lambda \rightarrow \infty$ in Fig. 2). Thus we make the use of explicit expressions Eq. 13 and Eq. 15 to analyze data on partially and homogeneously labeled polymers respectively. Practically, in both cases we tabulate $G_2(h_\perp^2)/G_2(0)$ for a wide range of $h_\perp^2$ as exemplified in Fig. 2 (curves for $\lambda = 0$ and $\lambda \rightarrow \infty$). We normalize the experimentally obtained correlation functions $G_2(t)$ by their plateau values. We use tabulated $G_2(h_\perp^2)/G_2(0)$ dependencies to find $h_\perp^2$ values corresponding to each measured data point $G_2(t)$. This gives the $h_\perp^2(t)$ dependence (and respectively $\langle \Delta r_\perp^2(t) \rangle = w_{xy}^2 h_\perp^2(t)$).

The extracted temporal dependencies of transverse monomer motion are presented in Fig. 5. Despite the difference in the temporal behavior of the original correlation functions for partially and homogeneously labeled filaments, the application of the appropriate expressions for each case leads to consistent data on monomers dynamics for both sets of measurements. The data span a wide range of time scales: from $\sim 40\mu s$ to $\sim 2s$.

In Fig. 5 we compare the experimental data to the predictions of two types of semi-flexible polymer dynamics theories, which do (14) and do not account for the hydrodynamic interactions (13). The measurements agree very well with the hydrodynamic theory over about four decades in time. The deviation of the data at long time scales is probably related to the diffusion of the filament as a whole.

To conclude, we adapt FCS formalism for the studies of the internal dynamics of semi-flexible polymers. We make use of a developed formalism to obtain non-invasive measurements on the kinetics of segmental motion in actin filaments. Two labeling strategies, local labeling and homogeneous labeling, lead to consistent results. The transverse segmental MSD $\langle \Delta r_\perp^2(t) \rangle$ is probed over a wide range of timescales, from $\sim 40\mu$s to ~ 2s. Almost over the whole range the data points follow closely the prediction of hydrodynamic theories (12, 14). Thus, non-invasive measurements of $\langle r^2(t) \rangle$ carried out with FCS allow us to test hydrodynamic theories directly over a wide temporal range. We note, finally, that although in the presented measurements the transverse motion is the dominant mode of motion, in other cases, such as F-actin in the presence of molecular motors (myosins) the longitudinal motion may be significant. Then the two suggested labeling strategies, partial and homogeneous labeling, being very different in their sensitivity to longitudinal motion, can be used in conjunction to separate transverse and longitudinal components of segmental displacement.

We are indebted to R. Granek, E. Frey and K. Kroy for fruitful discus-

References

1. Gittes, F., B. Mickey, J. Nettleton, and J. Howard. 1993. Flexural rigidity of microtubules and actin filaments measured from thermal fluctuations in shape. *J. Cell. Biol.* 120:923–934.

2. Piekenbrock, T., and E. Sackmann. 1992. Quasielastic light scattering study of thermal excitations of f-actin solutions and of growth kinetics of actin filaments. *Biopolymers* 32:1471–1489.

3. Kas, J., H. Strey, and E. Sackmann. 1994. Direct imaging of reptation for semiflexible actin filaments. *Nature* 368:226–229.

4. LeGoff, L., O. Hallatschek, E. Frey, and F. Amblard. 2002. Tracer studies on f-actin fluctuations. *Phys. Rev. Lett.* 89:258101.

5. Gisler, T., and D. A. Weitz. 1999. Scaling of the microrheology of semidilute f-actin solutions. *Phys. Rev. Lett.* 82:1606–1609.

6. Schmidt, F. G., B. Hinner, and E. Sackmann. 2000. Microrheometry underestimates the values of the viscoelastic moduli in measurements on f-actin solutions compared to macrorheometry. *Phys. Rev. E.* 61:5646–5653.

7. Caspi, A., M. Elbaum, R. Granek, A. Lachish, and D. Zbaida. 1998. Semiflexible polymer network: A view from inside. *Phys. Rev. Lett.* 80:1106–1109.

8. Xu, J. Y., A. Palmer, and D. Wirtz. 1998. Rheology and microrheology of semiflexible polymer solutions: Actin filament networks. *Macromol.* 31:6486–92.

9. Wong, I. Y., M. L. Gardel, D. R. Reichman, E. R. Weeks, M. T. Valentine, A. R. Bausch, and D. A. Weitz. 2004. Anomalous diffusion probes microstructure dynamics of entangled f-actin networks. *Phys. Rev. Lett.* 92:178101.

10. Allegra, G., and F. Ganazzoli. 1981. Configurations and dynamics of real chains. i. polyethylene. *J. Chem. Phys.* 74:1310–1320.

11. Farge, E., and A. C. Maggs. 1993. Dynamic scattering from semiflexible polymers. *Macromolecules* 26:5041–5044.

12. Harnau, L., R. G. Winkler, and P. Reineker. 1996. Dynamic structure factor of semiflexible macromolecules in dilute solution. *J. Chem. Phys.* 104:6355–6368.

13. Harnau, L., R. G. Winkler, and P. Reineker. 1997. Influence of stiffness on the dynamics of macromolecules in a melt. *J. Chem. Phys.* 106:2469–2476.

14. Granek, R. 1997. From semi-flexible polymers to membranes: Anomalous diffusion and reptation. *J. Phys. II (France)* 7:1761–1788.

15. Kroy, K., and E. Frey. 1997. Dynamic scattering from solutions of semiflexible polymers. *Phys. Rev. E* 55:3092–3101.

16. Morse, D. C. 1998. Viscoelasticity of tightly entangled solutions of semiflexible polymers. *Phys. Rev. E* 58:R1237–1240.

17. Gittes, F., and F. C. MacKintosh. 1998. Dynamic shear modulus of a semiflexible polymer network. *Phys. Rev. E* 58:R1241–1244.

18. Shusterman, R., S. Alon, T. Gavrinyov, and O. Krichevsky. 2004. Monomer dynamics in double- and single-standed dna polymers. *Phys. Rev. Lett.* 92:048303.

19. Lumma, D., S. Keller, T. Vilgis, and J. O. Radler. 2003. Dynamics of large semiflexible chains probed by fluorescence correlation spectroscopy. *Phys. Rev. Lett.* 90:218301.

20. Magde, D., E. Elson, and W. Webb. 1972. Thermodynamic fluctuations in a reacting system - measurement by fluorescence correlation spectroscopy. *Phys. Rev. Lett.* 29:705–708.

21. Elson, E. L., and D. Magde. 1974. Fluorescence correlation spectroscopy. i. conceptual basis and theory. *Biopolymers* 13:1–27.

22. Magde, D., E. L. Elson and W. W. Webb. 1974. Fluorescence correlation spectroscopy. i. an experimental realization. *Biopolymers* 13:29–61.

23. Haustein, E., and P. Schwille. 2003. Ultrasensitive investigations of biological systems by fluorescence correlation spectroscopy. *Methods* 29:153–166.

24. Thompson, N. L., A. M. Lieto, and N. W. Allen. 2002. Recent advances in fluorescence correlation spectroscopy. *Curr. Opin. Struct. Biol.* 12:634–641.

25. Rigler, R., and E. Elson, editors. 2001. Fluorescence correlation spectroscopy : theory and applications. Springer, Berlin and New York.

26. Krichevsky, O., and G. Bonnet. 2002. Fluorescence correlation spectroscopy: the technique and its applications. *Rep. Prog. Phys.* 65:251297.

27. Rigler, R., U. Mets, J. Widengren, and P. Kask. 1993. Fluorescence correlation spectroscopy with high count rate and low background: analysis of translational diffusion. *Europ. J. Biophys.* 22:169–175.

28. Bern, B. J., and R. Pecora. 1976. Dynamic Light Scattering. Wiley, New York.

29. Pardee, J. D., and J. A. Spudich. 1982. Purification of muscle actin. *Methods Enzymol.* 85:164–181.

30. Andrianantoandro, E., L. Blanchoin, D. Sept, J. A. McCammon, and T. D. Pollard. 2001. Kinetic mechanism of end-to-end annealing of actin filaments. *J. Mol. Biol.* 312:721–730.

31. Perret, E., A. Leung, A. Morel, H. Feracci, and P. Nassoy. 2002. Versatile decoration of glass surfaces to probe individual protein-protein interactions and cellular adhesion. *Langmuir.* 18:846–854.

Figure Legends

Figure 1.

Dependence of the apparent length of the labeled segment on its real length as given by Eq. 16 for $\omega = 5$ (close to the aspect ratio of the sampling volume in our setup). The lengths are given in the units of confocal volume radius $\lambda = L/w_{xy}$, $\lambda_{app} = L_{app}/w_{xy}$. The apparent length of very long $\lambda \gg 1$ segments approaches $\approx 2.5 w_{xy}$. *Inset:* Ratio of the apparent length to the real length of the labeled segment. Labeled segment lengths of $L < w_{xy}$ ($\lambda < 1$) results in $L_{app} \approx L$.

Figure 2.

Calculated dependencies of FCS correlation function on the transverse mean-square displacement of semi-flexible polymer segment. FCS correlation functions are normalized by their zero-time values (to have unit amplitude) and transverse MSD is given in the units of confocal volume radius $h_\perp^2 = \langle \Delta r_\perp^2 \rangle / w_{xy}^2$. The leftmost curve is given by standard FCS expression Eq. 14 for isotropic motion. The other curves are calculated from Eqs. 12, 13, 15 for different values of λ, *left to right:* 0, 1, 2, 5, 15, ∞. *Inset:* Same curves in semilog scale allowing to assess wider range of $h_\perp^2$.

Figure 3.

Photon count trace of partially labeled actin filaments (*Sample 1*). The photon trace is collected with 16.7ns resolution and split into 100ms bins. The data points represent photon counts per bin: (a) Full trace over the duration of one measurement, (b) Zoom into first 30s of measurement. Bursts (dotted line) due to the passage of labeled parts are separated by the intervals of background noise (solid line).

Figure 4.

Total $G_{tot}(t)$ (dotted line), background $G_b(t)$ (thin solid line) and signal $G(t)$ (thick solid line) correlation functions of partially labeled filaments (*Sample 1*). $G_{tot}(t)$ is obtained by analyzing the complete photon trace, $G_b(t)$ is caused by the diffusion of free fluorophore and is calculated from the photon trace in between the bursts in Fig. 3. $G(t) = G_{tot}(t) - G_b(t)$ is the correlation function resulting from the motion of F-actin labeled segments after background substraction. Dashed line is the correlation function of

homogeneously labeled actin (*Sample 2*) after subtraction of background noise. The correlation function of *Sample 2* was normalized to have the same amplitude as that of *Sample 1* in order to facilitate the comparison of temporal behavior.

Figure 5.

The kinetics of random motion $\langle \Delta r_\perp^2(t) \rangle$ of actin filaments' segments. Experimental measurements on locally labeled (thick dashed line) and on homogeneously labeled (thick solid line) are compared to the theoretical predictions by the hydrodynamic theory of Granek (14) (thin solid line) and non-hydrodynamic theory by Harnau et al (12) (thin dashed line). The parameters used for the calculation are $l_p = 17\mu m$, filament diameter of $7nm$, solvent viscosity $1mPa \cdot s$, and filament length of $6\mu m$.
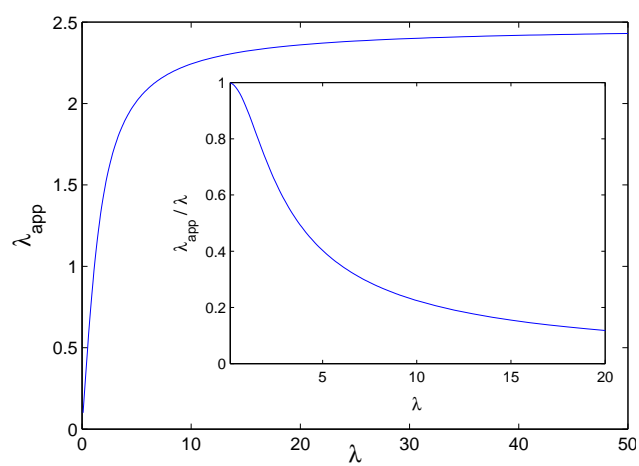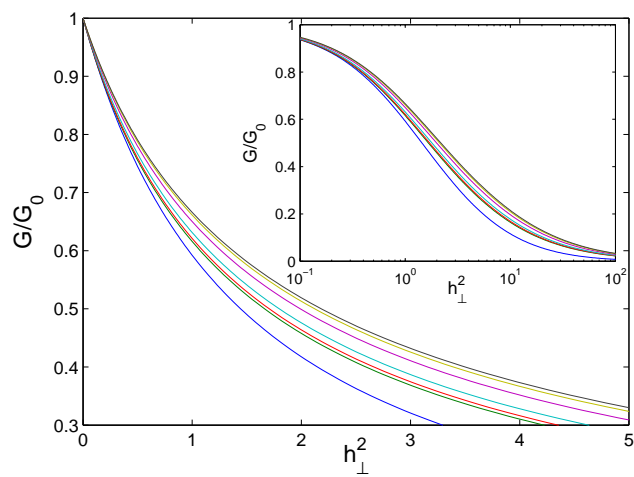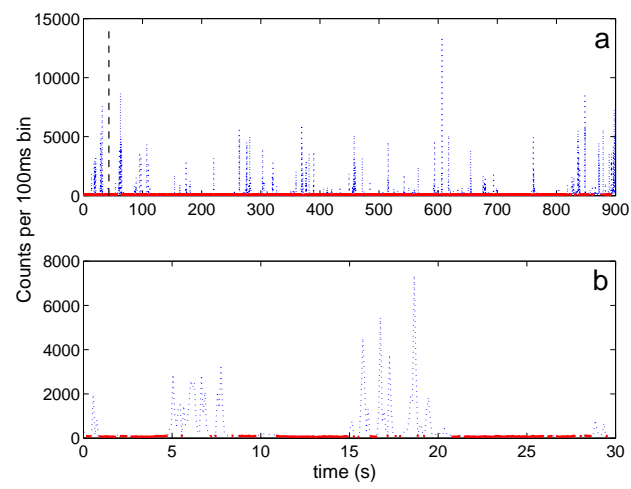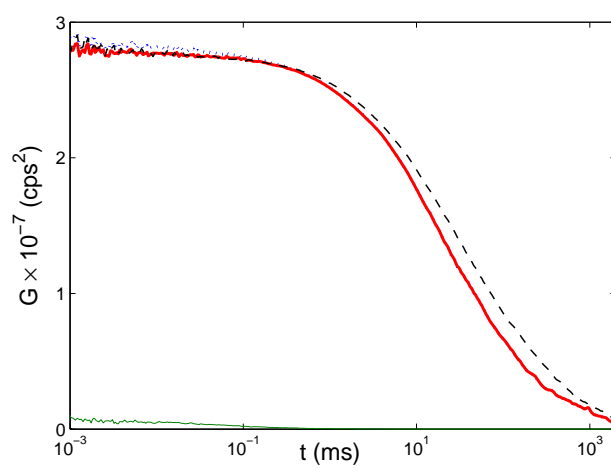
Figure 1:

Figure 2:

Figure 3:

Figure 4:

Figure 5: